

UNIVERSIDADE FEDERAL DE ALAGOAS
INSTITUTO DE CIÊNCIAS FARMACÊUTICAS – ICF
CURSO DE GRADUAÇÃO EM FARMÁCIA

Atividade antioxidante e antimicrobiana de nanopartículas de sílica
mesoporosa embebidas em própolis vermelha

Maceió, 2023

LAIS VANESSA DE AZEVEDO TELES DA SILVA

Atividade antioxidante e antimicrobiana de nanopartículas de sílica mesoporosa embebidas em própolis vermelha

Trabalho de conclusão de curso apresentado ao corpo docente do Instituto de Ciências Farmacêuticas da Universidade Federal de Alagoas como requisito parcial para a obtenção do título de bacharel em Farmácia. Orientador: Prof^o. Dr^o. Eduardo Jorge da Silva Fonseca.

MACEIÓ, 2023



**UNIVERSIDADE FEDERAL DE ALAGOAS
INSTITUTO DE CIÊNCIAS FARMACÊUTICAS
CURSO DE FARMÁCIA**

Campus A.C. Simões, Av. Lourival Melo Mota, s/n, Tabuleiro dos Martins
CEP:57072-900 Maceió – AL
Coordenação do curso de Farmácia
Telefone: (82) 3214.1170; e-mail: tccfarmaciaufal@gmail.com



**FICHA PARA AVALIAÇÃO DE ARTIGO CIENTÍFICO/CAPÍTULO DE LIVRO COMO
TRABALHO DE CONCLUSÃO DE CURSO (TCC)**

Aluna: Laís Vanessa de Azevedo Teles da Silva

Artigo científico intitulado Antioxidant and antimicrobial activity of propolis embedded mesoporous silica nanoparticles

Campo reservado para ARTIGO

Nome da revista onde foi aceito artigo: DRUG DEVELOPMENT AND INDUSTRIAL PHARMACY

ISSN da revista: 1520-5762

Fator de impacto ou Qualis da revista: QUALIS A3 (QUADRIÊNIO 2017-2020 CAPES)

DOI do artigo: <https://doi.org/10.1080/03639045.2020.1782423>

Campo reservado para atribuição de nota pela Banca Avaliadora

Avaliador 1: Prof. Dr. Valter Alvino



Documento assinado digitalmente

VALTER ALVINO DA SILVA
Data: 10/05/2023 15:13:38-0300
Verifique em <https://validar.iti.gov.br>

Assinatura do avaliador 1:

Avaliador 2: Prof. Dr. João Xavier de Araújo Júnior



Documento assinado digitalmente

JOAO XAVIER DE ARAUJO JUNIOR
Data: 10/05/2023 20:43:20-0300
Verifique em <https://validar.iti.gov.br>

Assinatura do avaliador 2:

Nota do TCC: 10,0

Data: 10/05/2023



Documento assinado digitalmente

EURICA ADELIA NOGUEIRA RIBEIRO
Data: 10/05/2023 21:47:04-0300
Verifique em <https://validar.iti.gov.br>

Assinatura a coordenadora de TCC:

RESEARCH ARTICLE

Antioxidant and antimicrobial activity of red propolis embedded mesoporous silica nanoparticles

Laís F. Azevedo de M. Oliveira^a , Laís Vanessa de Azevedo Teles da Silva^b, Ticiano G. do Nascimento^b , Lara Mendes de Almeida^b , Rodrigo José Nunes Calumby^b , Ábner Magalhães Nunes^c , Leonardo Mendonça Tenório de Magalhães Oliveira^d  and Eduardo J. da Silva Fonseca^a 

^aLaboratory of Characterization and Microscopy of Materials, Institute of Physics, Postgraduate Program in Materials Sciences, Center of Technology, Federal University of Alagoas (UFAL), Maceió, Brazil; ^bInstitute of Pharmaceutical Sciences, Quality Control Laboratory of Drugs and Medicines, Federal University of Alagoas (UFAL), Maceió, Brazil; ^cCatalysis and Chemical Reactivity Group, Institute of Chemistry and Biotechnology (IQB), Federal University of Alagoas (UFAL), Maceió, Brazil; ^dProcess Laboratory, Technology Center, Federal University of Alagoas (UFAL), Maceió, Brazil

ABSTRACT

This work brings the promise of MCM-41 mesoporous silica as a vehicle for red propolis for the development of controlled release drugs and delivery to a specific target site. The synthesis of MCM-41 by the sol-gel method with a pore size of approximately 3.6 nm and the incorporation of red propolis extract by the physical adsorption method in ethanolic medium were easily accomplished with around 15% encapsulation. MCM-41 and MCM-41 with red propolis (MCM-41/Pr) were characterized by Fourier transform infrared spectroscopy, X-ray diffraction, thermal analysis, N₂ adsorption-desorption, scanning electron microscopy, and an ultra-high-performance liquid chromatography-diode array detection (UPLC-DAD). *In vitro* release of encapsulated red propolis was analyzed in phosphate buffer at pH 7.2, 7.4, and 7.6. An *in vitro* test for MCM-41/Pr antioxidant activity was performed using 2,2-diphenyl-1-picrylhydrazyl as well as analysis of antibacterial activity against *Staphylococcus aureus* by the well diffusion method. UPLC-DAD analysis showed that the integrity of the red propolis constituents was maintained after the embed process, and the antioxidant and antibacterial activities were preserved.

ARTICLE HISTORY

Received 13 February 2020
Revised 31 May 2020
Accepted 9 June 2020

KEYWORDS

Synthesis; nanostructures; mesoporous; red propolis extract; UPLC-DAD; antibacterial activities

Introduction

Medical interest in nanotechnology has expanded in recent decades. Mesoporous silica nanoparticles (MSNs) have attracted a lot of attention since the introduction of M41S class materials by the scientists of Mobil Corporation [1]. MCM-41, one of the members of this class, has a uniform hexagonal array of one-dimensional mesoporous channels with a pore diameter in the range of 2–50 nm in accordance with IUPAC recommendations [2,3]. Furthermore, the literature reports several advantages with the use of silica nanoparticles, such as high surface area [3], facile functionalization [4–6], adjustable pore size, which can be loaded with bioactive molecules imparting additional stability by safeguarding them against degradation [7], and excellent monodispersity [8,9].

In the last decades, many researchers have synthesized MSNs with various morphologies, dimensions, and pore sizes for use in countless applications [10]. Mesoporous silica can be easily obtained using the sol-gel method in the presence of assembled cationic surfactant micelle templates [11–13], which serve as structure-directing agents for polymerizing the silica component by electrostatic interaction [14]. The synthesis of MSNs can be achieved by various adjustments to the synthesis parameters, including the pH of the reaction mixture, reaction time, stirring rate, characteristics of the surfactants, concentration and the source of silica [15].

Integration between materials science, nanotechnology, and medicine has favored the manufacture of a variety of multifunctional nanomaterials for numerous applications; for example, the encapsulation of propolis in polymeric nanosystems for the purpose of treating leishmaniasis [16]. Other studies report the use of mesoporous silica in several biology-relevant fields/nanomedicine, including cell imaging [17], diagnosis [18,19], bio-analysis [20], antimicrobial and antifungal activity [21] and drug delivery with low solubility and bioavailability to minimize adverse effects and increase the efficacy of the drug [22]. Moreover, these materials are highly desirable due to chemical [23] and thermal stability and great biocompatibility. Thus, the use of these mesoporous nanoparticles can improve the bioavailability of lipophilic substances, as is the case with most natural products [24–27].

The use of medicinal plants, phytotherapy products, and opotherapy products has been attracting interest from the scientific community as a result of recent scientific evidence of their beneficial pharmacologic properties as anti-inflammatory, anticancer, antioxidant, antibacterial, antiviral, antiparasitic, and antifungal agents [16,28–33]. Propolis is a complex resinous substance collected by bees (*Apis mellifera*) [34–37] from different parts of plants. This product is used by bees as a natural barrier against insects, invading microorganisms, and in beehive repair [38,39].

Red propolis is classified as a group 13 propolis and has been shown to have several biological properties such as antibacterial [40], antiparasitic [16], antioxidant [31], and anticancer [37]. In

Brazil, red propolis can be found in different Brazilian states and, as a result of factors such as climate, environmental conditions, and biodiversity, different chemical compounds are found in its structure [41–43]. More than 300 components have been reported in red propolis samples analyzed by diverse techniques [44]. The most important classes of pharmacologically active compounds in red propolis are flavonoids, isoflavonoids, phenolic acid, terpenes, xanthenes, propolones, and guttiferones [40,45–48]. With this composition rich in resins and waxes, propolis has low solubility and bioavailability and this disadvantage can be overcoming with a nanosystem loader.

The present study aims to establish the antioxidant and anti-microbial activities of red propolis after undergoing the adsorption process on MCM-41 MSNs. The purpose of encapsulation is to overcome the disadvantages of propolis related to its low availability and solubility.

Materials and methods

Materials

Red propolis material (90 mL, 11% w/v) was purchased from the O Cortiço apiary (Maceió, Brazil). Tetraethyl orthosilicate (TEOS) 99% and *n*-cetyl-*n,n,n*-trimethyl ammonium bromide (CTAB) were purchased from Sigma-Aldrich (St. Louis, MO). Ammonium hydroxide (NH₄OH, 25–28 wt%) was purchased from Laboratory of Nanosystems Technology Active Substance Carriers (TecNano, UFAL, Porto Alegre, Brazil). HPLC grade acetonitrile and methanol were purchased from J.T. Baker Mallinckrodt-Avantor (Phillipsburg, NJ).

Methods

Synthesis of MCM-41

MCM-41 samples were prepared according to the procedure of Gan et al. [15] by the co-condensation method using TEOS as the silica source and CTAB as a template, with minor modification. First, 500 mL of deionized water was heated to 50 °C until stability was reached. Then, 26.4 mL of NH₄OH (28.7 wt%) was added to adjust the pH to approximately 11; 0.56 g of CTAB was added. The solution was stirred for 15 min for complete homogenization. Then, 2.9 mL of TEOS was added dropwise under magnetic stirring for 2 h at 50 °C. The resulting solution was centrifuged at 8000 rpm for 5 min and washed twice with ultrapure water and ethanol until the pH was neutral and then dried at 80 °C overnight. To remove the CTAB template, the solution was calcined under atmospheric air at 550 °C for 4 h at a heating rate of 5 °C min⁻¹ to obtain MCM-41.

Red propolis loading on mesoporous silica nanoparticles (MCM-41/Pr)

Red propolis (250 mg) was dispersed in 2.5 mL of absolute ethanol, and 100 mg of MCM-41 was added to this solution. The suspension was maintained under ultrasonic stirring for 30 min at 40 °C and kept at rest for 24 h at 40 °C. The solution was then centrifuged under the same conditions as previously, and the nanoparticles were collected and dried at room temperature.

Characterization

Fourier transform infrared spectroscopy analysis

Fourier transform infrared (FTIR) spectroscopy of the red propolis, MCM-41, and MCM-41/Pr were measured using an FTIR Analysis Instrument (Model IRPretige-21, Shimadzu, Kyoto, Japan) with KBr

pellets in the 400–4000 cm⁻¹ region, with a resolution of 4 cm⁻¹, by accumulating 120 scans, and the band intensities were expressed as transmittance (%), a technique used to identify the structural characteristics of organic and inorganic samples from the absorption bands in the infrared region [49].

X-ray diffraction analysis

Small-angle X-ray diffraction (XRD) was used to obtain information on the pore architecture of mesoporous structures and to determine the crystallographic arrangements, symmetry, and phase purity. The analysis was performed using XRD analysis instruments (Model Diffractometer XRD-6000, Shimadzu, Kyoto, Japan). The sample was mounted on holders and then introduced for analysis, scanned within the 2θ range of 1–70; the source consisted of CuKα₁ radiation (λ = 1.79 Å), monochromator on secondary optics, 30 kV power, and 30 mA current at a scan speed of 2° min⁻¹ and a step size of 0.02°.

Thermogravimetry

Thermogravimetry (TG) of the red propolis, MCM-41, and MCM-41/Pr was performed using a differential scanning calorimeter (Model TGA 50, Shimadzu, Tokyo, Japan), with a mass of 5.0 mg ± 10% in a hermetically sealed platinum pan. The heating rate was 10 °C min⁻¹ in the range from 30 °C to 900 °C under an atmosphere of nitrogen and a flow rate of 50 mL min⁻¹.

Brunauer–Emmett–Teller/Barrett–Joyner–Halenda analyses

The surface areas were calculated by Brunauer–Emmett–Teller (BET) analysis in the *P/P*₀ relative range of 0.01–1.0 for the pore size distributions. Pore volume was obtained by the Barrett–Joyner–Halenda (BJH) method and the nitrogen adsorption–desorption isotherms of the MCM-41 and MCM-41/Pr samples were obtained using a NOVA 2200e surface area and pore size analyzer (Quantachrome Instruments, Boynton Beach, FL) at –196 °C. Before the analysis, 0.1 g of the samples was heat treated at 70 °C under vacuum for 5 h.

Scanning electron microscopy

The morphological structure and size particles of MCM-41 and MCM-41/Pr were identified by scanning electron microscopy (SEM; Model Superscan SSX-550, Shimadzu, Kyoto, Japan), operating in backscatter mode at an acceleration voltage of 10.0 kV. Before observation, the samples were prepared in hydroalcoholic solution (80%), placed in the sample port, and dried; however, they were coated with a thin layer of gold.

Ultra-high-performance liquid chromatography–diode array detection

The identification and quantification of flavonoids in red propolis extract and MCM-41/Pr in solid state were performed using ultra-high-performance liquid chromatography–diode array detection (UPLC-DAD; Shimadzu, Kyoto, Japan) with a high-pressure pump module (Model LC-20ADXR), degasser (Model DGU-20A3R), module auto-injector (Model SIL-20AXR), module oven chromatograph column, photodiode array detectors (Model EPDM-20A), module fluorescence detector (Model RF-20A), and controller (Model CBM-20A). The separation of flavonoids was performed using a reversed-phase column (C₁₈, 150 × 4.6 mm; 5 μm). For the mobile phase, MilliQ water was used as solvent A and acetonitrile as solvent B,

pumped at a flow rate of 0.3 mL min⁻¹ flow rate. The analytical methodology was followed according to Azevedo et al. [16].

The identification and quantification of red propolis in the MCM-41 was measured by the retention time of six markers (liquiritigenin, isoliquiritigenin, formononetin, biochanin A, pinocembrin, and pinobanksin) present in the red propolis extract and related to the calibration curve of these patterns traced in previous studies [16]. Then, 100 mg of ethanol red propolis extract was solubilized in 10 mL of absolute ethanol in an ultrasonic bath for 10 min to obtain a concentration of 10 mg mL⁻¹. From this, a stock solution was prepared to a concentration of 1 mg mL⁻¹. The solution was filtered using 0.22- μ m syringe filter (K18-230) papers, and 2 μ L of solution at a concentration of 310 μ g mL⁻¹ was injected into the UPLC system. The same procedure was repeated for MCM-41/Pr.

In vitro red propolis release

MCM-41/Pr (17 mg) was dispersed in 50 mL of phosphate-buffered saline (PBS) solution with different pH values (5.5, 7.2, 7.4, and 7.6) and used to evaluate the *in vitro* release of MCM-41/Pr. The assay was performed for 24 h under stirring at 100 rpm, keeping the temperature constant at 37 °C \pm 1 °C. Samples were taken at time intervals of 15 min, 30 min, 45 min, 1 h, 1.5 h, 2 h, 3 h, 4 h, 8 h, 12 h, and 24 h. After collecting 1 mL of PBS solution at the mentioned times, the nanoparticles were separated from the solution by centrifugation for 5 min at 10,000 rpm. The release of red propolis from the pores of MCM-41 to PBS was monitored by UV-vis spectrophotometry (Model UV-1280, Shimadzu, Kyoto, Japan) at a wavelength of 280 nm. The trials were performed in rejoinder.

Before the *in vitro* release assay, a calibration curve for the red propolis extract was made. This allowed the absorbance value to be related to the concentration of the analyte in the solution through a linear equation. The calibration curve was prepared with triplex red propolis extract at concentrations of 70, 60, 50, 40, 30, 20, 10, and 5 μ g mL⁻¹ ($r^2=0.9991$). Absorbance values were measured in a UV-vis spectrophotometer at 280 nm wavelength.

Two models were used to adjust the experimental kinetic data and try to explain the mechanism of drug release: Pseudo-first order model, proposed by Lagergren and Pseudo-second order model, projected by Ho and McKay. The determination coefficient (R^2) and the average relative error (ARE) were used to measure the reliability of the models. The pseudo-first order equation is [50]:

$$q_t = q_e(1 - e^{-k_1 t}) \quad (1)$$

where k_1 is the pseudo-first order red propolis release rate constant (h⁻¹); q_e (μ g/mL) and q_t (μ g/mL) are the amounts of red propolis released per mL of the equilibrated buffer solution and in a specific time, respectively; and t is the process time. The pseudo-second order equation is [50]:

$$q_t = \frac{k_2 q_e^2 t}{1 + k_2 q_e t} \quad (2)$$

where k_2 is the pseudo-second order red propolis release rate constant (mL/ μ g.h).

The first model suggests that the rate of solute release is proportional to the number of active sites present in the structure of the silica nanoparticle, indicating that such interaction is reversible. The second model proposes that the bioactive liberation capacity is directly proportional to the number of active sites occupied in the mesoporous silica nanostructure. In addition, they also suggest

the presence of chemical interactions, indicating some difficulty in reversibility [50].

In vitro biological activity

Antioxidant activity of the red propolis and MCM-41/Pr using the DPPH method

Quantitative assessment of the antioxidant activity of red propolis and MCM-41/Pr was performed according to the methods described in the literature [51] with some modifications. The antioxidant activity was measured by the inhibition of free radical 2,2-diphenyl-1-picrylhydrazyl (DPPH) and monitored by obtaining the absorbance values of solutions of the samples at different concentrations. The equation used to calculate the antioxidant activity is

$$\text{Antioxidant activity (\%)} = 100 - \frac{\text{ABS}_{\text{sample}} - \text{ABS}_0}{\text{ABS}_{\text{Control}}} \times 100 \quad (3)$$

where $\text{ABS}_{\text{sample}}$ is the absorbance of the sample solution with DPPH, ABS_0 is the absorbance of the sample without DPPH, and $\text{ABS}_{\text{Control}}$ is the absorbance of the DPPH solution.

The DPPH solution (3 mM) was prepared using 0.005 g of DPPH reagent and was solubilized in a 100-mL volumetric flask with absolute ethanol. The red propolis and MCM-41/Pr were prepared at an initial concentration of 1.0 mg mL⁻¹ red propolis in ethanol as solvent. Aliquots of 500, 375, 250, 125, 50, 25, 5, and 2.5 μ L were transferred to 5-mL volumetric flasks, and then 2.0 mL of DPPH solution (3 mM) was added and diluted with ethanol until final concentrations of 100, 75, 50, 25, 10, 5, 1, and 0.5 μ g mL⁻¹ were achieved, respectively. The reaction took place in a dark room at 25 °C for 30 min. The absorbance readings were performed with a spectrophotometer (Model UV-1280, Shimadzu, Kyoto, Japan) at 518 nm wavelength. Absolute ethanol was used to prepare control solutions.

Assessment of the antibacterial activity of MCM-41/Pr and red propolis extract

The antimicrobial activity of MCM-41/Pr and red propolis extract was determined using the well diffusion method with diameter of \sim 8 mm. This method is similar to the disk diffusion method and is widely used for the analysis of antibacterial activity of natural or related products [52]. *Staphylococcus aureus* ATCC 25923 strain was used to verify the sensitivity profile of the MCM-41/Pr and the red propolis extracts at concentrations of 150, 225, 375, 500, 750, and 1050 μ g mL⁻¹ in dimethyl sulfoxide. This strain of *S. aureus* was previously cultured on brain heart infusion agar for 18–24 h at 37 °C \pm 1 °C, and a colony was removed from this culture for the preparation of a McFarland 0.5 suspension in Müeller-Hinton broth. About 300 μ L of the suspension of different concentrations of MCM-41/Pr and red propolis extract was inoculated into wells previously prepared in Müeller-Hinton agar plates. Halo size readings were performed after incubation of the plates for 18–24 h at 37 °C \pm 1 °C.

Results and discussion

Fourier transform infrared spectroscopy

The structure characteristics of the red propolis extract, MCM-41, and MCM-41/Pr obtained by the FTIR method are shown in Figure 1. The spectrum of red propolis shows a band of absorption at 3336 cm⁻¹, characteristic of the vibration of an O-H group typical of phenolic compounds (Figure 1, spectrum 1), which are prevalent in

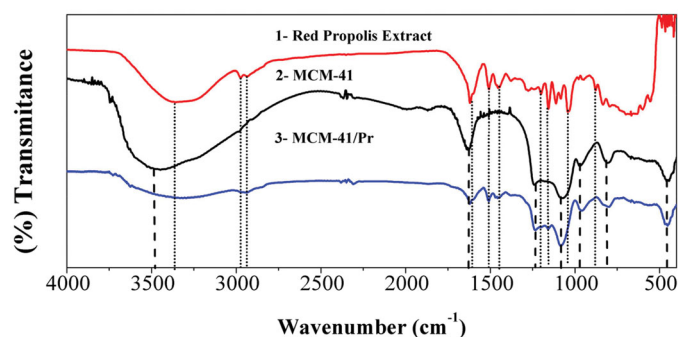


Figure 1. FTIR of the (1) red propolis extract, (2) MCM-41, and (3) MCM-41/Pr.

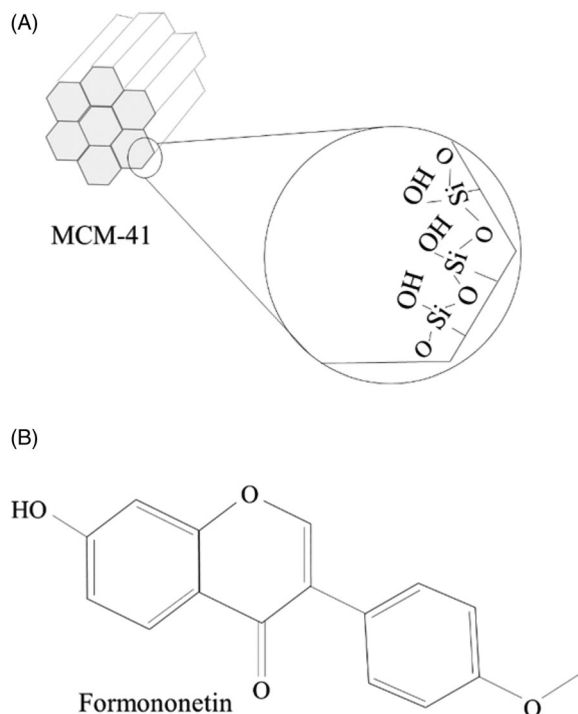


Figure 2. Structure of (A) MCM-41 and (B) phenolic compounds of the red propolis extract.

red propolis [16]. Bands of absorption at 2970 cm^{-1} and 2932 cm^{-1} correspond to axial deformation of CH_3 groups. The bands of absorption at 1617 cm^{-1} , 1496 cm^{-1} , and 1450 cm^{-1} are due to stretching of $\text{C}=\text{C}$ groups in aromatic rings. Bands at 1160 cm^{-1} and 1200 cm^{-1} correspond to vibration of $\text{C}-\text{O}$ groups in phenols. The band at 1045 cm^{-1} corresponds to vibration of a $\text{C}-\text{O}$ ether bond, and the band at 877 cm^{-1} can be attributed to angular deformation outside the plain of $\text{C}-\text{H}$ aromatic compounds.

The FTIR spectrum of MCM-41 (Figure 1, spectrum 2) shows an absorption band in the wavenumber region at 3450 cm^{-1} , characterizing stretching of hydrogen bonds $\text{O}-\text{H}$ present in the molecular structure of MCM-41 (Figure 2(A)). The wavenumber region at 1625 cm^{-1} can be attributed to angular vibrations of molecules of water. The bands in the wavenumber regions at 1240 cm^{-1} and 1076 cm^{-1} show asymmetrical stretching of the $\text{Si}-\text{O}-\text{Si}$ group, and the band at 953 cm^{-1} can be attributed to symmetrical stretching of the $\text{Si}-\text{O}-\text{Si}$ group. The band at 812 cm^{-1} corresponds to stretching of the silanol group $\text{Si}-\text{OH}$, and the band at 450 cm^{-1} is characteristic of $\text{O}-\text{Si}-\text{O}$ group vibrations.

Figure 1 (spectrum 3) shows the sample of MCM-41/Pr with absorption bands characteristic of MCM-41, but with significant

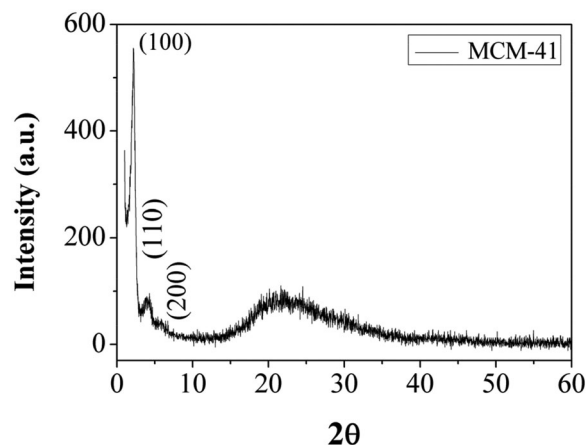


Figure 3. X-ray diffraction of MCM-41.

reduction in the wavenumber intensity at 3450 cm^{-1} , probably due to interaction of hydrogen bonds with hydroxyls present in the silica (Figure 2(A)) and the hydroxyls present in the phenolic compounds of propolis (Figure 2(B)). In addition, the presence of absorption bands can be seen at 2970 cm^{-1} , 2932 cm^{-1} , 1627 cm^{-1} , 1508 cm^{-1} , 1450 cm^{-1} , and 1157 cm^{-1} , which are characteristics of the molecular phenolic compounds in red propolis. The absorption bands at 1240 cm^{-1} , 1076 cm^{-1} , 953 cm^{-1} , 812 cm^{-1} , and 450 cm^{-1} correspond to the molecular structure of MCM-41, indicating that red propolis was incorporated in MCM-41 without damaging its structure.

X-ray diffraction

XRD of MCM-41 (Figure 3) shows the absence of peaks at higher angles, such as 15° to 50° , because the structural wall of MCM-41 is formed of amorphous silica. However, a strong diffraction Bragg peak at a low angle (100) at $2\theta = 2.28^\circ$ and two weaker peaks at higher angles (110) and (200) at $2\theta = 4.15^\circ$ and $2\theta = 5.77^\circ$ can be seen, representing the hexagonal structure $p6mm$ in an ordered manner where one pore is surrounded by another six.

Thermogravimetry

Figure 4 (curve 1) shows the thermal decomposition analysis of MCM-41. The graph presents the mass loss at only one point between 80°C and 100°C , corresponding to the endothermic reaction. Loss of approximately 32.64% of adsorbed water in the pores of the nanostructure can be observed. The thermogravimetric curve of the red propolis extract (Figure 4, curve 2) shows three mass decay points: (i) the first decay point between 100°C and 120°C due to dehydration; (ii) a second decay point between 120°C and 135°C from the melting process of compounds of low molecular weight such as flavonoids, isoflavonoids, and other phenolic compounds; (iii) a third point between 220°C and 450°C attributed to decarboxylation of the remaining organic material can still be seen [16]. The TG curve of MCM-41/Pr (Figure 4, curve 3) shows the first decay event around 80°C , equivalent to approximately 13.56% water loss. Then, two decay events occur equivalent to the decomposition of red propolis observed in the previous thermogram. Approximately, 14.56% mass loss occurs up to 550°C . After encapsulation, the temperature at which propolis deteriorates was higher, demonstrating better physicochemical stability of the bioactive.

Brunauer–Emmett–Teller/Barrett–Joyner–Halenda analyses

Figure 5(A,B) shows the nitrogen adsorption–desorption isotherms of the samples of MCM-41 and MCM-41/Pr, respectively. The isothermal formats can be used to classify porosity and pore size, according to IUPAC. Both isotherms showed characteristics typical of mesoporous materials, type IV, with pore size between 2 and 50 nm. In addition, the hysteresis curve type H1 corresponds to homogeneous organization of the pore grid.

The results calculated from the adsorption/desorption isotherm curves by the BET method are set out in Table 1.

MCM-41 had a high surface area ($1289.97 \text{ m}^2 \text{ g}^{-1}$). After the addition of propolis, this surface area reduced by more than half (Table 1). MCM-41 showed a pore volume of 0.450 mL g^{-1} and, in turn, the MCM-41/Pr sample showed a pore volume of 0.320 mL g^{-1} , a reduction equivalent to approximately 28.89% of the pore volume. These facts can be attributed to the incorporation of propolis into the pores of the mesoporous particles. Both curves had a mean pore diameter of 3.63 nm.

Scanning electronic microscopy

Figure 6 shows the SEM of MCM-41 (Figure 6(A)) and MCM-41/Pr (Figure 6(B)) obtained at a magnification of $15,000\times$ and $18,000\times$ (scale bars, $1 \mu\text{m}$), respectively. The photomicrographs show the particles size between 100 and 300 nm with spherical formation. The particles tend to come together to form an agglomerated

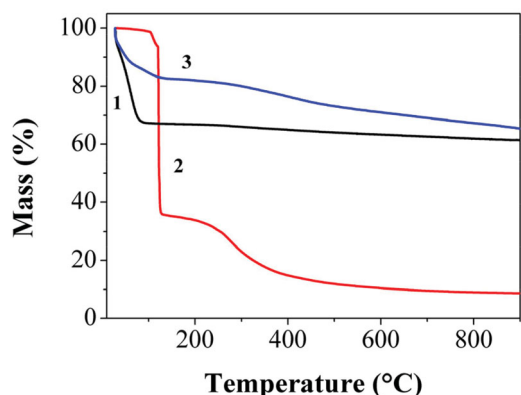


Figure 4. Thermogravimetric analysis of (1) MCM-41, (2) red propolis extract, and (3) MCM-41/Pr.

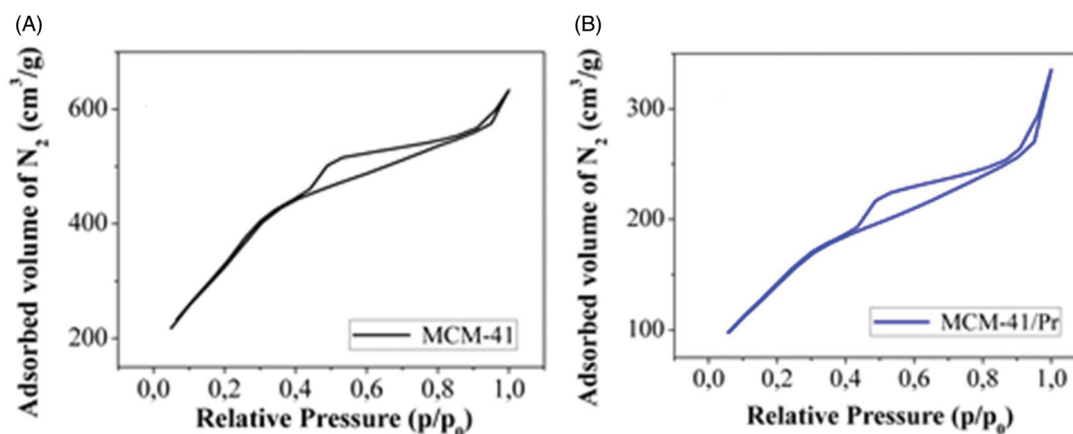


Figure 5. Nitrogen adsorption–desorption isotherms of (A) MCM-41 and (B) MCM-41/Pr.

structure affecting the uniform distribution of the final size. This probably occurs due to the difficulty of controlling the nucleation rate and growth of the center formed initially [53]. According to Wu et al. [3], the morphology and particle size depend as much on the kinetics of sol–gel chemistry as the reaction temperature, pH, and concentrations of water, surfactant, and silica precursor. However, the adsorption process of the propolis extract occurred effectively. Removal of CTAB by the calcination method may also have influenced the non-uniform distribution of the final particle size. Nevertheless, internalization of the propolis extract occurred, reaching about 15% (p/p) incorporation, as seen in Section ‘Thermogravimetry’ (Figure 4, curve 3).

UPLC-DAD

The chromatograms in Figure 7 show the identification of flavonoids and isoflavonoids present in the red propolis extract (Figure 7(A)) and MCM-41/Pr (Figure 7(B)): (1) liquiritigenin (12.29 min), (2) daidzein (12.46 min), (3) pinobanksin (15.96 min), (4) isoliquiritigenin (16.97 min), (5) formononetin (17.87 min), (6) pinocembrin (22.37 min), and (7) biochanin A (23.18 min). The red propolis extract and MCM-41/Pr yield times were similar to the retention times of the analytical standards used in the development of the chromatographic method.

Table 2 shows the concentration of the seven markers present in red propolis extract and MCM-41/Pr with intermediary precision. The red propolis extract shows 2.94, 6.51, 5.80, 9.92, 0.74, 1.59, and $0.87 \mu\text{g mL}^{-1}$ for daidzein, liquiritigenin, isoliquiritigenin, formononetin, biochanin A, pinocembrin, and pinobanksin, respectively. Following the same sequence, the seven markers show the following concentrations for MCM-41/Pr: 3.33, 7.41, 6.12, 11.44, 0.75, 1.60, and $0.99 \mu\text{g mL}^{-1}$. The analyses were done at $500 \mu\text{g mL}^{-1}$ for red propolis extract and MCM-41/Pr. After incorporation of red propolis extract into the carrier system (MCM-41), the physicochemical properties of propolis remained the same.

Table 1. Structural data for the MCM-41 and MCM-41/Pr samples.

Sample	S_{BET} ($\text{m}^2 \text{ g}^{-1}$)	Pore size _{BHJ} (nm)	V_t ($\text{cm}^3 \text{ g}^{-1}$)
MCM-41	1289.971	3.638	0.450
MCM-41/Pr	549.228	3.606	0.320

S_{BET} : specific surface area; V_t : total pore volume.

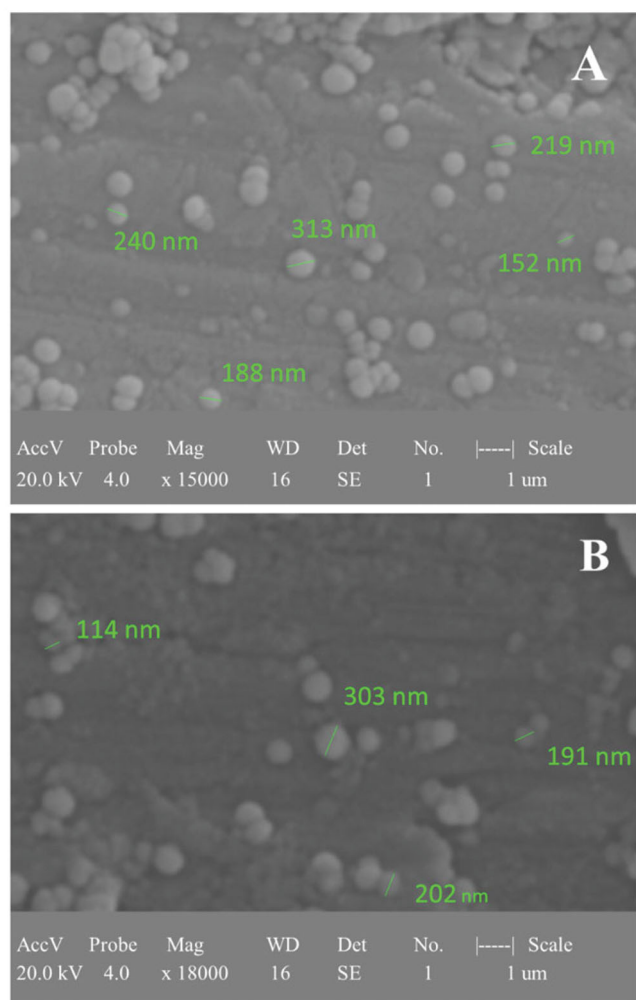


Figure 6. SEM of (A) MCM-41 and (B) MCM-41/Pr.

In vitro red propolis release

The release of red propolis from MCM-41 *in vitro* can be seen in Figure 8. Dissolution assays were conducted using slightly alkaline and acidic conditions. At pH 5.5, approximately $5.76 \mu\text{g mL}^{-1}$ of the red propolis extract was released in the medium in the first hours, reaching $7.78 \mu\text{g mL}^{-1}$ (15%) after 24 h. For all the alkaline pH conditions studied, the initial percentage release of red propolis extract was around 25%, equivalent to about $13 \mu\text{g mL}^{-1}$. However, at pH 7.4 and 7.6, the amount of red propolis in the dissolution medium, approximately $20 \mu\text{g mL}^{-1}$ (40%) after 4 h, reaching approximately $21 \mu\text{g mL}^{-1}$ (42%) after 24 h of dissolution. For pH 7.2, the release was around $17 \mu\text{g mL}^{-1}$ (35%) and $18 \mu\text{g mL}^{-1}$ (37%), respectively, for the times 4 and 24 h.

For a better understanding of the mechanism for releasing the propolis extract from the silica nanoparticles, the experimental data were adjusted to two mathematical models: pseudo-first order and pseudo-second order. Considering the data in Table 3, it is noted that the kinetic models of pseudo-first and pseudo-second order obtained good adjustments for all the pHs studied, since the coefficient of determination was above 0.86.

Observing the response only for the pseudo-first order model, it is perceived that it is difficult to represent the attenuated dissolution rate that occurs at pHs of 5.5, 7.2, and 7.4 between 0 and 5 h, establishing a trend agreement only after this period. However, as the pH rises, the initial dissolution rate increases, leading to better convergence in this region. However, it is at

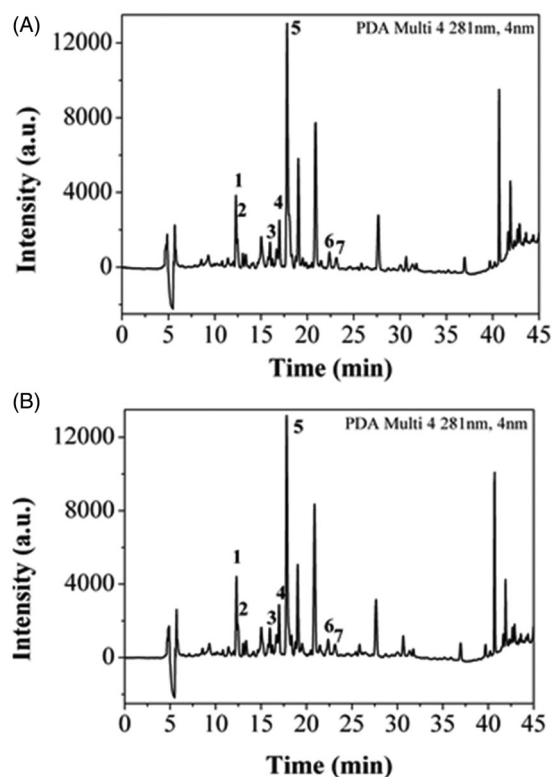


Figure 7. Chromatographic profile of Brazilian red propolis extract using UPLC-DAD for (A) red propolis extract and (B) MCM-41/Pr. (1) Liquiritigenin (12.29 min), (2) daidzein (12.46 min), (3) pinobanksin (15.96 min), (4) isoliquiritigenin (16.97 min), (5) formononetin (17.87 min), (6) pinocembrin (22.37 min), and (7) biochanin A (23.18 min).

Table 2. Determination of markers present in red propolis extract and MCM-41/Pr.

	Red propolis extract	MCM-41/Pr ($\mu\text{g mL}^{-1}$)
Daidzein	2.941	3.329
Liquiritigenin	6.508	7.411
Isoliquiritigenin	5.798	6.117
Formononetin	9.923	11.438
Biochanin A	0.736	0.749
Pinocembrin	1.586	1.592
Pinobanksin	0.872	0.985

pH 5.5 that the best adjustment occurs, with R^2 of 0.9554 and $ARE = 6.45\%$.

According to the answers for the pseudo-second order model, it was observed that it presented a lower mean relative error in relation to the adjustment in all pHs of the pseudo-second order model, even managing to better represent the attenuated dissolution rate between 0 and 5 h. In addition, this model was the one that best approximated the value of the experimental equilibrium dissolution, with an ARE for this point of 4.38% and in all analyses, while the pseudo-first order was 9.58%.

According to Oliveira et al. [50], the pseudo-first order model suggests the presence of mostly physical interactions, while the pseudo-second order would indicate a greater contribution of chemical interactions. Thus, it can be inferred that the interactions described in the dissolution process would have a higher energy than electrical interactions, explaining the difficulty of responding to the pseudo-first order model for the first hours of the process.

Furthermore, noting that the most coherent adjustments considering both models, occurred for pHs of 7.6, this can confirm

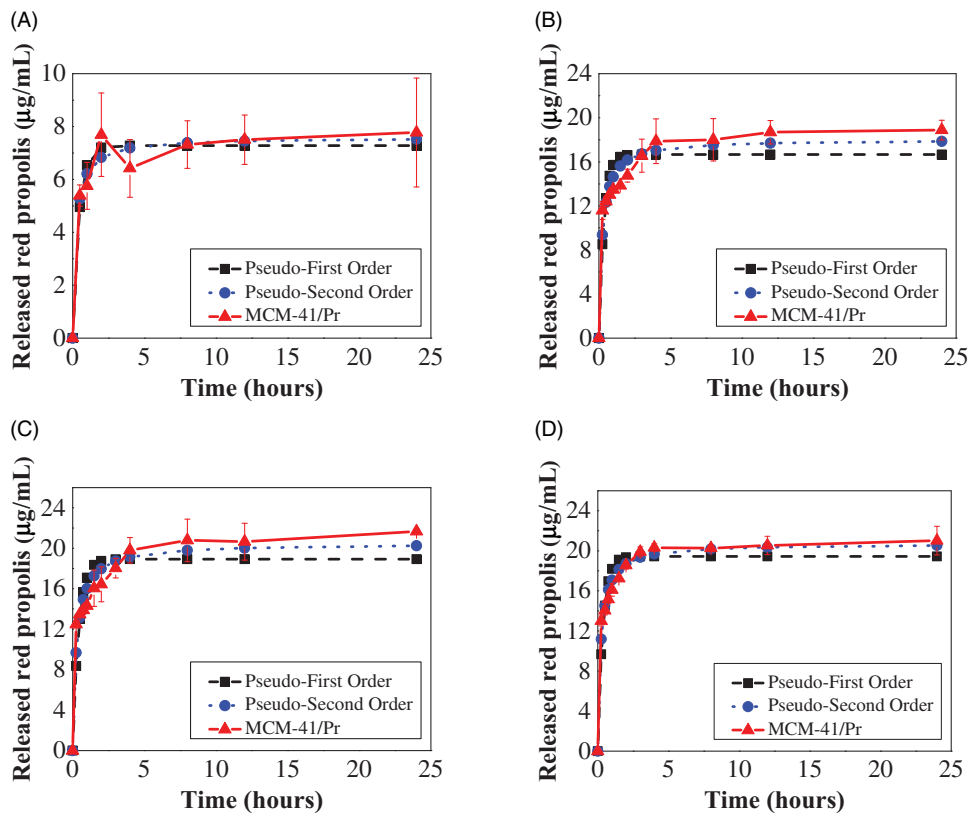


Figure 8. *In vitro* release of red propolis flavonoids from MCM-41 at pH of 5.5, 7.2, 7.4, and 7.6.

Table 3. *In vitro* released kinetics of red propolis embedded MCM-41.

Sample	pH	Pseudo-first order $q_t = q_e(1 - e^{-k_1 t})$				Pseudo-second order $q_t = \frac{k_2 q_e^2 t}{1 + k_2 q_e t}$			
		R^2	ARE (%)	q_e ($\mu\text{g mL}^{-1}$)	k_1 (1 h^{-1})	R^2	ARE (%)	q_e ($\mu\text{g mL}^{-1}$)	k_2 ($\text{mL } \mu\text{g}^{-1} \text{ h}^{-1}$)
MCM-41/Pr	5.5	0.9554	6.45	7.28	2.2855	0.9649	5.51	7.59	0.5951
	7.2	0.8659	11.54	16.67	2.8657	0.9488	6.88	18.03	0.2398
	7.4	0.8626	12.34	18.93	2.3284	0.9475	7.51	20.49	0.1746
	7.6	0.9263	8.45	19.43	2.7549	0.9806	4.15	20.72	0.2267

that the optimal pH of the dissolution phenomenon will revolve around this value. Confirming that the best bioavailability of propolis occurs in more alkaline media, since the flavonoids present in greater amounts in red propolis are considered weak acids and have better solubility at more basic pH, allowing easier dissociation of the silica surface.

Diseased cells need a more alkaline medium than healthy cells (pH 7.2) for their metabolism to function properly. Thus, the bioavailability of propolis for these cells tends to be greater than for healthy cells. Since, under these conditions, the propolis flavonoids that are considered weak acids have better solubility at more basic pH, allowing easier dissociation of the silica surface.

Antioxidant activity of the red propolis and MCM-41/Pr

Table 4 shows that red propolis extract and MCM-41/Pr at low concentrations (10, 5, 1, and $0.5 \mu\text{g mL}^{-1}$) presented similar antioxidant activity with significant differences at a p value $<.05$. For concentrations greater than or equal to $25 \mu\text{g mL}^{-1}$, significant differences can be observed at a p value $<.001$. In addition, MCM-41/Pr presented a lower antioxidant activity than red propolis extract, nevertheless showing a satisfactory result

Table 4. Antioxidant activity (%) of red propolis extract and MCM-41/Pr.

Concentration ($\mu\text{g mL}^{-1}$)	Antioxidant activity (%)	
	Red propolis extract	MCM-41/Pr
100	$93.26 \pm 2.17^{**}$	$91.82 \pm 0.95^{**}$
75	$92.68 \pm 0.18^{**}$	$87.53 \pm 0.17^{**}$
50	$92.00 \pm 0.15^{**}$	$85.38 \pm 0.23^{**}$
25	$81.92 \pm 0.93^{**}$	$71.37 \pm 1.74^{**}$
10	$48.26 \pm 1.38^*$	$38.60 \pm 1.48^*$
5	$28.97 \pm 1.54^*$	$23.18 \pm 0.91^*$
1	$8.66 \pm 0.58^*$	$6.27 \pm 2.00^*$
0,5	$3.35 \pm 2.58^*$	$3.30 \pm 0.45^*$

Significant difference between red propolis extract and MCM-41/Pr at concentrations (100, 75, 50, 25, 10, 5, 1, and $0.5 \mu\text{g mL}^{-1}$) with $^{**}p < .05$ and $^*p < .001$ using the Bonferroni post-test from the two-way ANOVA test.

against free radicals. The EC_{50} (effective concentration at which the DPPH radicals were scavenged by 50%) of the scavenging effect of free radicals was $11.60 \mu\text{g mL}^{-1}$ for red propolis extract and $14.59 \mu\text{g mL}^{-1}$ for MCM-41/Pr. The results showed that MCM-41 has potential as a carrier of flavonoids, isoflavonoids, and other compounds present in red propolis extract, because the physicochemical integrity of the pharmacological properties is retained.

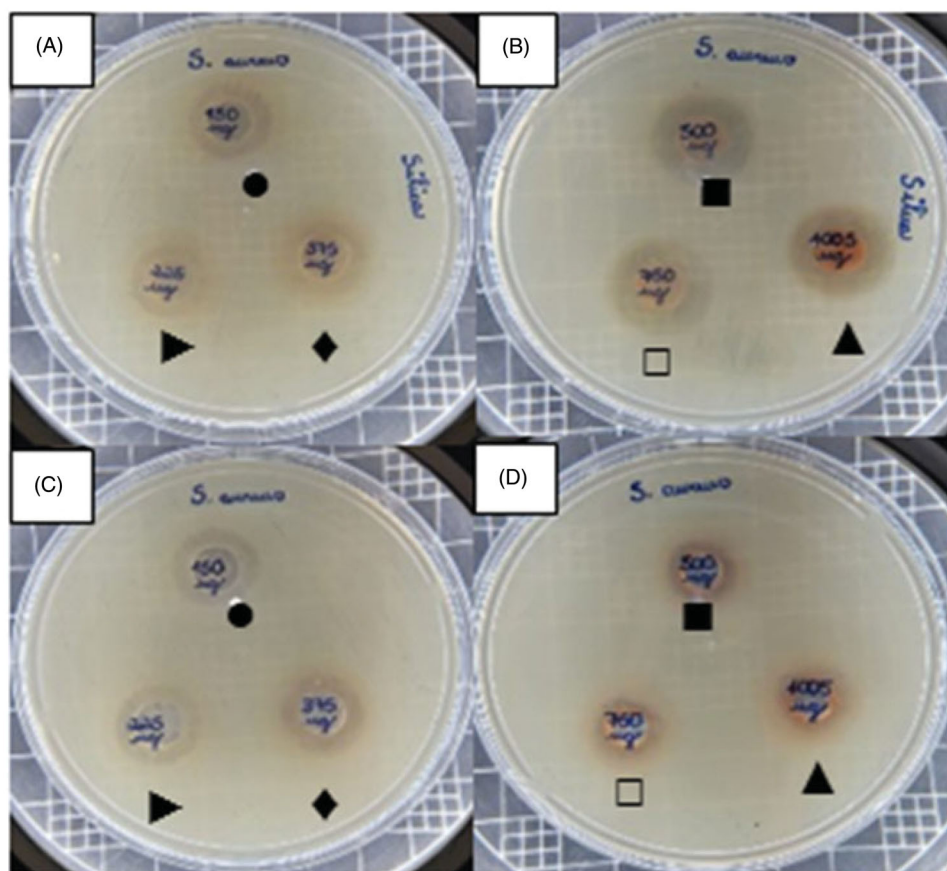


Figure 9. Antimicrobial activity of MCM-41/Pr (A, B) and red propolis extract (C, D) against *S. aureus* (ATCC 25923) well diffusion method. In the following concentrations: (●) $150 \mu\text{g mL}^{-1}$, (▶) $225 \mu\text{g mL}^{-1}$, (◆) $375 \mu\text{g mL}^{-1}$, (◻) $500 \mu\text{g mL}^{-1}$, (◀) $750 \mu\text{g mL}^{-1}$, and (▲) $1050 \mu\text{g mL}^{-1}$.

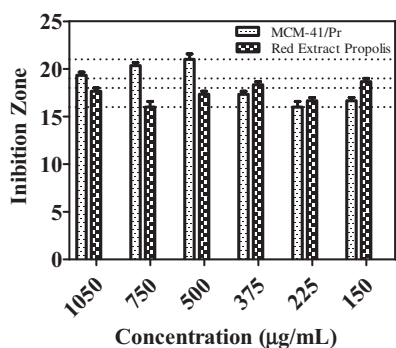


Figure 10. Graphic antimicrobial activity of MCM-41/Pr and red propolis extract against *S. aureus* (ATCC 25923) well diffusion method.

Assessment of antibacterial activity of MCM-41/Pr and red propolis extract

The results of the well diffusion method showed that the inhibition zones obtained with MCM-41/Pr (Figure 9(A,B)) and red propolis extract (Figure 9(C,D)) against the *S. aureus* bacterial strain ATCC 25923 showed significant differences between the two different types of treatment with a p value of .0002 (Figure 10). MCM-41/Pr tested at concentrations of 1050, 750, 500, 375, 225, and $150 \mu\text{g mL}^{-1}$ revealed an inhibition zone of, approximately, 19, 20, 21, 17, 16, and 17 mm in diameter, respectively (Figure 9(A,B)). Red propolis extract at the same concentrations had an inhibition zone of, approximately, 18, 16, 17, 18, 17, and 20 mm, respectively (Figure 9(C,D)). Observing the statistical data, it can be concluded that the antimicrobial activity between the different

concentrations shows significant differences presenting a p value less than .0001 (Figure 10). At concentrations greater than $500 \mu\text{g mL}^{-1}$, the MCM-41/Pr showed better performances compared to the free extract. Probably due to the preservation of the physicochemical properties of propolis when reversed by nanoparticles, combined with the gradual release of the nanostructure.

Conclusions

The present study reports the antioxidant and antimicrobial activities of red propolis extract embedded in MCM-41 type nanoparticles, which showed better performances. The synthesis by the sol-gel method was easily reproduced, and a hexagonal p6mm nanostructure was obtained with a pore size of 3.63 nm and particle size between 100 and 300 nm. In addition, the surface area reached was satisfactory, reducing by approximately half after incorporation of the red propolis extract. It was possible to observe the presence of approximately 15% red propolis extract in the MCM-41 through TG analysis and pore volume reduction (BJH). FTIR analysis showed that the MCM-41 structure was maintained after incorporation of red propolis extract as well as adsorptive interaction between MCM-41 and red propolis. UPLC-DAD analysis showed that the stability and physicochemical properties of red propolis extract were maintained. In conclusion, MSNs are a potential structure for carrying propolis extract because the active biological properties of red propolis are maintained. These results may prove useful in developing oral, injectable, or tablet medicines. There is still the possibility of investment in directional studies in the area of cosmetics.

Acknowledgements

The authors thank Professor PhD Irinaldo Diniz Basílio Júnior of Laboratory of Technology and Control of Drugs, Institute of Pharmaceutical Science, UFAL; Professor PhD Mario Roberto Meneghetti; and Professor PhD Simoni Margareti Plentz Meneghetti of Catalysis and Chemical Reactivity Group, Institute of Chemistry and Biotechnology (IQB) to UFAL.

Disclosure statement

No potential conflict of interest was reported by the author(s).

Funding

The authors would like to thank Federal University of Alagoas (UFAL), CAPES, and CNPq for financial support. This study was also supported by Professor PhD Antonio Osimar Sousa da Silva of Synthesis of Catalyst Laboratory (LSCat), UFAL.

ORCID

Láís F. Azevedo de M. Oliveira  <http://orcid.org/0000-0003-4915-1750>

Ticiano G. do Nascimento  <http://orcid.org/0000-0002-3856-8764>

Lara Mendes de Almeida  <http://orcid.org/0000-0002-9027-5221>

Rodrigo José Nunes Calumby  <http://orcid.org/0000-0002-2313-5552>

Ábner Magalhães Nunes  <http://orcid.org/0000-0002-4909-9713>

Leonardo Mendonça Tenório de Magalhães Oliveira  <http://orcid.org/0000-0002-5709-1375>

Eduardo J. da Silva Fonseca  <http://orcid.org/0000-0001-5975-2467>

Data availability statement

The raw/processed data required to reproduce these findings cannot be shared at this time as the data also form part of an ongoing study.

References

- [1] Beck JS, Vartuli JC, Roth WJ, et al. A new family of mesoporous molecular sieves prepared with liquid crystal templates. *J Am Chem Soc.* 1992;114(27):10834–10843.
- [2] Slowing II, Vivero-Escoto JL, Trewyn BG, et al. Mesoporous silica nanoparticles: structural design and applications. *J Mater Chem.* 2010;20(37):7924–7937.
- [3] Wu S-H, Mou C-Y, Lin H-P. Synthesis of mesoporous silica nanoparticles. *Chem Soc Rev.* 2013;42(9):3862–3875.
- [4] Saroj S, Rajput SJ. Tailor-made pH-sensitive polyacrylic acid functionalized mesoporous silica nanoparticles for efficient and controlled delivery of anti-cancer drug etoposide. *Drug Dev Ind Pharm.* 2018;44(7):1198–1211.
- [5] Szegedi A, Popova M, Goshev I, et al. Controlled drug release on amine functionalized spherical MCM-41. *J Solid State Chem.* 2012;194:257–263.
- [6] Kermannezhad K, Najafi Chermahini A, Momeni MM, et al. Application of amine-functionalized MCM-41 as pH-sensitive nano container for controlled release of 2-mercaptobenzoxazole corrosion inhibitor. *Chem Eng J.* 2016;306:849–857.
- [7] Popova M, Szegedi A, Yoncheva K, et al. New method for preparation of delivery systems of poorly soluble drugs on the basis of functionalized mesoporous MCM-41 nanoparticles. *Microporous Mesoporous Mater.* 2014;198:247–255.
- [8] Tang F, Li L, Chen D. Mesoporous silica nanoparticles: synthesis, biocompatibility and drug delivery. *Adv Mater.* 2012; 24(12):1237–1504.
- [9] Lu J, Liong M, Li Z, et al. Biocompatibility, biodistribution, and drug-delivery efficiency of mesoporous silica nanoparticles for cancer therapy in animals. *Small.* 2010;6(16):1794–1805.
- [10] Zhao L, Qin H, Wu R, et al. Recent advances of mesoporous materials in sample preparation. *J Chromatogr A.* 2012; 1228:193–204.
- [11] Dubey RS, Rajesh Y, More MA. Synthesis and characterization of SiO₂ nanoparticles via sol-gel method for industrial applications. *Mater Today Proc.* 2015;2(4–5):3575–3579.
- [12] Yang B, Chen Y, Shi J. Mesoporous silica/organosilica nanoparticles: synthesis, biological effect and biomedical application. *Mater Sci Eng R Rep.* 2019;137:66–105.
- [13] Croissant JG, Cattoën X, Man WCM, et al. Syntheses and applications of periodic mesoporous organosilica nanoparticles. *Nanoscale.* 2015;7(48):20318–20334.
- [14] Lv X, Zhang L, Xing F, et al. Controlled synthesis of monodispersed mesoporous silica nanoparticles: particle size tuning and formation mechanism investigation. *Microporous Mesoporous Mater.* 2016;225:238–244.
- [15] Gan Q, Zhu J, Yuan Y, et al. A dual-delivery system of pH-responsive chitosan-functionalized mesoporous silica nanoparticles bearing BMP-2 and dexamethasone for enhanced bone regeneration. *J Mater Chem B.* 2015;3(10):2056–2066.
- [16] Azevedo LF, Da Silva PF, Brandão MP, et al. Polymeric nanoparticle systems loaded with red propolis extract: a comparative study of the encapsulating systems, PCL-Pluronic versus Eudragit®E100-Pluronic. *J Apicult Res.* 2018; 57(2):255–270.
- [17] Tang L, Cheng J. Nonporous silica nanoparticles for nanomedicine application. *Nano Today.* 2013;8(3):290–312.
- [18] Fathi M, Majidi S, Zangabad PS, et al. Chitosan-based multifunctional nanomedicines and theranostics for targeted therapy of cancer. *Med Res Rev.* 2018;38(6):2110–2136.
- [19] Lee JE, Lee N, Kim T, et al. Multifunctional mesoporous silica nanocomposite nanoparticles for theranostic applications. *Acc Chem Res.* 2011;44(10):893–902.
- [20] Solanki P, Patel S, Devkar R, et al. Camptothecin encapsulated into functionalized MCM-41: in vitro release study, cytotoxicity and kinetics. *Mater Sci Eng C Mater Biol Appl.* 2019;98:1014–1021.
- [21] Makvandi P, Ghaemy M, Ghadiri AA, et al. Photocurable, antimicrobial quaternary ammonium-modified nanosilica. *J Dent Res.* 2015;94(10):1401–1407.
- [22] Lin L, Tang F, Liu H, et al. *In vivo* delivery of silica nanoparticle encapsulated docetaxel for liver cancer therapy with low toxicity and high efficacy. *ACS Nano.* 2010;4(11):6874–6882.
- [23] Croissant JG, Fatieiev Y, Almalik A, et al. Mesoporous silica and organosilica nanoparticles: physical chemistry, biosafety, delivery strategies, and biomedical applications. *Adv Healthcare Mater.* 2018;7(4):1700831.
- [24] Bharti C, Gulati N, Nagaich U, et al. Mesoporous silica nanoparticles in target drug delivery system: a review. *Int J Pharm Investig.* 2015;5(3):124–133.

- [25] Simovic S, Ghouchi-Eskandar N, Moom Sinn A, et al. Silica materials in drug delivery applications. *Curr Drug Discov Technol.* 2011;8(3):269–276.
- [26] Wang Y, Zhao Q, Han N, et al. Mesoporous silica nanoparticles in drug delivery and biomedical applications. *Nanomedicine.* 2015;11(2):313–327.
- [27] Tarn D, Ashley CE, Xue M, et al. Mesoporous silica nanoparticle nanocarriers: biofunctionality and biocompatibility. *Acc Chem Res.* 2013;46(3):792–801.
- [28] Yuan H, Ma Q, Ye L, et al. The traditional medicine and modern medicine from natural products. *Molecules.* 2016; 21(5):559.
- [29] Arif T, Bhosale JD, Kumar N, et al. Natural products – antifungal agents derived from plants. *J Asian Nat Prod Res.* 2009;11(7):621–638.
- [30] Cui PH, Duke CC. Chemical classification and chemistry of phytotherapeutics constituents. In: Ramzan, Iqbal, editor. *Phytotherapies: efficacy, safety, and regulation.* 1st ed. John Wiley & Sons, Inc; 2015. p. 199–235.
- [31] Do Nascimento TG, Da Silva PF, Azevedo LF, et al. Polymeric nanoparticles of Brazilian red propolis extract: preparation, characterization, antioxidant and leishmanicidal activity. *Nanoscale Res Lett.* 2016;11(1):301.
- [32] Gandhi GR, Barreto PG, Lima BS, et al. Medicinal plants and natural molecules with in vitro and in vivo activity against rotavirus: a systematic review. *Phytomedicine.* 2016; 23(14):1830–1842.
- [33] Araujo MAR, Libério SA, Guerra RNM, et al. Mechanisms of action underlying the anti-inflammatory and immunomodulatory effects of propolis: a brief review. *Rev Bras Farmacogn.* 2012;22(1):208–219.
- [34] Ghisalberti EL. Propolis: a review. *Bee World.* 1979;60(2):59–84.
- [35] Bogdanov S. Propolis: composition, health, medicine: a review. *Bee Prod Sci.* 2017;1:1–44.
- [36] López BGC, Schmidt EM, Eberlin MN, et al. Phytochemical markers of different types of red propolis. *Food Chem.* 2014;146:174–180.
- [37] De Mendonça ICG, Porto I, Do Nascimento TG, et al. Brazilian red propolis: phytochemical screening, antioxidant activity and effect against cancer cells. *BMC Complement Altern Med.* 2015;15:357.
- [38] Simone-Finstrom M, Spivak M. Propolis and bee health: the natural history and significance of resin use by honey bees. *Apidologie.* 2010;41(3):295–311.
- [39] Bankova V. Chemical diversity of propolis and the problem of standardization. *J Ethnopharmacol.* 2005;100(1–2):114–117.
- [40] Righi AA, Alves TR, Negri G, et al. Brazilian red propolis: unreported substances, antioxidant and antimicrobial activities. *J Sci Food Agric.* 2011;91(13):2363–2370.
- [41] Alencar SM, Oldoni TLC, Castro ML, et al. Chemical composition and biological activity of a new type of Brazilian propolis: red propolis. *J Ethnopharmacol.* 2007;113(2):278–283.
- [42] Cabral ISR, Oldoni TLC, Prado A, et al. Composição fenólica, atividade antibacteriana e antioxidante da própolis vermelha brasileira [Phenolic composition, antibacterial and antioxidant activity of Brazilian red propolis]. *Quím Nova.* 2009;32(6):1523–1527.
- [43] Devequi-Nunes D, Machado BAS, Barreto GA, et al. Chemical characterization and biological activity of six different extracts of propolis through conventional methods and supercritical extraction. *PLoS One.* 2018;13(12):e0207676.
- [44] Freires IA, De Alencar SM, Rosalen PL. A pharmacological perspective on the use of Brazilian red propolis and its isolated compounds against human diseases. *Eur J Med Chem.* 2016;110:267–279.
- [45] Rufatto LC, Dos Santos DA, Marinho F, et al. Red propolis: chemical composition and pharmacological activity. *Asian Pac J Trop Biomed.* 2017;7(7):591–598.
- [46] Piccinelli AL, Lotti C, Campone L, et al. Cuban and Brazilian red propolis: botanical origin and comparative analysis by high-performance liquid chromatography–photodiode array detection/electrospray ionization tandem mass spectrometry. *J Agric Food Chem.* 2011;59(12):6484–6491.
- [47] Silva FRG, Matias TMS, Souza LIO, et al. Phytochemical screening and in vitro antibacterial, antifungal, antioxidant and antitumor activities of the red propolis Alagoas. *Braz J Biol.* 2019;79(3):452–459.
- [48] Da Silva SS, Thomé GDS, Cataneo AHD, et al. Brazilian propolis antileishmanial and immunomodulatory effects. *Evid Based Complement Altern Med.* 2013;2013:1–7.
- [49] Pavia PL, Lampman GM, Kriz GS, et al. *Introduction to spectroscopy.* 4th ed. Boston (MA): Cengage Learning; 2013.
- [50] Oliveira L, Oliveira L, Sonsin AF, et al. Ultrafast diesel oil spill removal by fibers from silk-cotton tree: characterization and sorption potential evaluation. *J Clean Prod.* 2020;263:1–13.
- [51] Brand-Williams W, Cuvelier ME, Berset C. Use of a free radical method to evaluate antioxidant activity. *LWT Food Sci Technol.* 1995;28(1):25–30.
- [52] Balouiri M, Sadiki M, Ibensouda SK. Methods for in vitro evaluating antimicrobial activity: a review. *J Pharm Anal.* 2016; 6(2):71–79.
- [53] Shaw DJ. In: Maar JH, translator. *Introduction to colloid and surface chemistry.* São Paulo: Edgard Blücher; 1975.